Cell

Identification of MOAG-4/SERF as a Regulator of Age-Related Proteotoxicity

Tjakko J. van Ham,[1,5,6] Mats A. Holmberg,[1,5] Annemieke T. van der Goot,[1,5] Eva Teuling,[1,5] Moises Garcia-Arencibia,[2] Hyun-eui Kim,[3] Deguo Du,[4] Karen L. Thijssen,[1] Marit Wiersma,[1] Rogier Burggraaff,[1] Petra van Bergeijk,[1] Jeroen van Rheenen,[1] G. Jerre van Veluw,[1,7] Robert M.W. Hofstra,[1] David C. Rubinsztein,[2] and Ellen A.A. Nollen[1,*]

[1]Department of Genetics, University Medical Centre Groningen, University of Groningen, Hanzeplein 1, 9700 RB Groningen, the Netherlands
[2]Cambridge Institute for Medical Research, Department of Medical Genetics, University of Cambridge Wellcome Trust/MRC Building, Addenbrooke's Hospital, Hills Road, Cambridge CB2 0XY, UK
[3]The Salk Institute for Biological Studies, Molecular and Cell Biology Laboratory, 10010 North Torrey Pines Road, La Jolla, CA 92037, USA
[4]Departments of Chemistry and Molecular and Experimental Medicine and The Skaggs Institute of Chemical Biology, The Scripps Research Institute, 10550 North Torrey Pines Road, La Jolla, CA 92037, USA
[5]These authors contributed equally to this work
[6]Present address: Cardiovascular Research Center, Massachusetts General Hospital, Harvard Medical School, 149 13th Street, Charlestown, MA 02129, USA
[7]Present address: Department of Biology, University of Utrecht, Padualaan 8, 3584 CH Utrecht, the Netherlands
*Correspondence: e.a.a.nollen@medgen.umcg.nl
DOI 10.1016/j.cell.2010.07.020

SUMMARY

Fibrillar protein aggregates are the major pathological hallmark of several incurable, age-related, neurodegenerative disorders. These aggregates typically contain aggregation-prone pathogenic proteins, such as amyloid-beta in Alzheimer's disease and alpha-synuclein in Parkinson's disease. It is, however, poorly understood how these aggregates are formed during cellular aging. Here we identify an evolutionarily highly conserved modifier of aggregation, MOAG-4, as a positive regulator of aggregate formation in *C. elegans* models for polyglutamine diseases. Inactivation of MOAG-4 suppresses the formation of compact polyglutamine aggregation intermediates that are required for aggregate formation. The role of MOAG-4 in driving aggregation extends to amyloid-beta and alpha-synuclein and is evolutionarily conserved in its human orthologs SERF1A and SERF2. MOAG-4/SERF appears to act independently from HSF-1-induced molecular chaperones, proteasomal degradation, and autophagy. Our results suggest that MOAG-4/SERF regulates age-related proteotoxicity through a previously unexplored pathway, which will open up new avenues for research on age-related, neurodegenerative diseases.

INTRODUCTION

Fibrillar aggregates of aggregation-prone proteins are a hallmark of several aging-associated neurodegenerative disorders, including Parkinson's, Huntington's, and Alzheimer's diseases (Chiti and Dobson, 2006; Goedert and Spillantini, 2006;

Scherzinger et al., 1997; Spillantini and Goedert, 2000). These aggregates typically contain amyloid-like fibrils composed of disease-specific aggregation-prone proteins, such as mutant huntingtin protein in Huntington's disease and alpha-synuclein in Parkinson's disease. The role of these aggregates in disease is still controversial: whereas the aggregates were initially thought to be pathogenic, more recent studies suggest that they have a protective role (Arrasate et al., 2004; Nagai et al., 2007; Sanchez et al., 2003; Saudou et al., 1998; Schaffar et al., 2004; Caughey and Lansbury, 2003; Haass and Selkoe, 2007; Kayed et al., 2003). Aggregation properties do appear to be required for pathogenesis, however, because inhibition of intramolecular aggregation and oligomerization suppresses toxicity (Nagai et al., 2007; Sanchez et al., 2003; Saudou et al., 1998; Schaffar et al., 2004). Thus, microscopically invisible, soluble, misfolded monomers and oligomeric precursors of aggregates are proposed as pathogenic structures (Nagai et al., 2007; Sanchez et al., 2003; Saudou et al., 1998; Schaffar et al., 2004).

The current view of how cells cope with misfolded and aggregation-prone proteins is that they are either refolded by molecular chaperones or degraded by the proteasome and other proteases (Ravikumar et al., 2004; Rubinsztein, 2006; Bukau et al., 2006; Goldberg, 2003). When these quality control mechanisms are overwhelmed or functionally impaired, which may occur in response to environmental stresses, during aging, and in disease, cells are thought to protect themselves against toxicity by sequestering aggregation-prone proteins, compactly folded, in aggregates (Hsu et al., 2003; Kaganovich et al., 2008; Kopito, 2000; Muchowski et al., 2002; Nollen et al., 2001; Williams and Paulson, 2008; Yamamoto et al., 2000).

How protein aggregates are formed and how this process is influenced by cellular aging and hereditary factors is unknown. One previously identified genetic suppressor of protein aggregation that links the process of aging and polyglutamine aggregation in a *C. elegans* model for disease is the longevity gene *age-1* (Morley et al., 2002). AGE-1 is a PI3 kinase in the

insulin/IGF-1-like signaling (IIS) pathway, which negatively regulates downstream transcription factors DAF-16/FOXO and HSF1 (Hsu et al., 2003; Morley and Morimoto, 2004; Ogg et al., 1997; Tissenbaum and Ruvkun, 1998). Reduced activity of the IIS pathway leads to activation of DAF-16 and HSF-1, which drive expression of a variety of longevity-promoting genes, including molecular chaperones with a role in preventing protein misfolding and aggregation (Cohen et al., 2006; Cohen and Dillin, 2008).

With *C. elegans* models for protein conformational diseases and genome-wide RNAi screens for genetic modifiers of protein aggregation, we have previously identified genes encoding proteins with roles in protein synthesis, protein folding, protein degradation, and vesicle trafficking and genes encoding proteins with no predicted function that when depleted increase the number of aggregates. These screens have revealed that a complex network of processes is involved in maintaining protein homeostasis (Nollen et al., 2004; van Ham et al., 2008). These modifiers include proteins with a confirmed role in modifying the toxicity of aggregation-prone proteins in human cell models, including HSP70 and cytosolic chaperonins (Behrends et al., 2006; Kitamura et al., 2006; Muchowski et al., 2000; Tam et al., 2006). These findings have indicated the evolutionary conservation of these protein quality control pathways and have exemplified the strength of using *C. elegans* to find genetic modifiers that may be relevant for human neurodegenerative diseases.

Here, we performed a chemical mutagenesis screen for genes encoding proteins with the opposite function, which upon mutation suppress protein aggregation. We identified *modifier of aggregation 4* (MOAG-4), which is homologous to SERF1A and SERF2 in humans. Our results suggest that inactivation of MOAG-4 suppresses proteotoxicity via a previously unexplored pathway.

RESULTS

Loss of *moag-4* Suppresses Polyglutamine Aggregation

To identify genes involved in the formation of aggregates, we used a *C. elegans* model for protein conformational diseases. This model expresses a polypeptide of 40 glutamine residues fused to yellow fluorescent protein (Q40::YFP), hereafter referred to as Q40 animals (Morley et al., 2002). One previously identified suppressor of protein aggregation in *C. elegans* is a loss-of-function mutation in the life-span-regulating gene *age-1* (Morley et al., 2002). We found that *age-1(hx546)*, hereafter referred to as *age-1* mutant, suppressed aggregation of Q40::YFP by 30% (Figure 1A).

We mutagenized Q40 animals to screen for *modifiers of aggregation (moag)* that showed suppression of aggregation similar or stronger than in *age-1* mutant animals and identified *moag-4 (pk2185)*, hereafter referred to as *moag-4* point mutant, which showed a 75% reduction in the number of aggregates (Figures 1A and 1E). The mutation in *moag-4* mapped to the gene Y37E3.4 (accession number: NM_058523) (Figure 1B), which encodes a small protein of unknown function that is evolutionarily highly conserved (Figure 1C). MOAG-4 (accession number: NP_490924) contains a 4F5 domain of unknown function. It is

predicted to have a helix-loop-helix secondary structure (Figure S1 available online). Although MOAG-4 has an abundance of positively charged amino acid residues, which is common for DNA- or RNA-binding domains, the DISIS algorithm suggests that interactions with nucleic acids are unlikely, although these cannot be excluded (Ofran et al., 2007; Ofran and Rost, 2003). The G210A mutation is a missense mutation in a strongly conserved amino acid residue, changing methionine at position 49 into an isoleucine (M49I) (Figure 1C). Human orthologs of MOAG-4 are SERF1A (accession number: NP_001171558) and SERF2 (accession number: AAC63516), which show 50% and 54% amino acid similarity to MOAG-4. These human orthologs are predicted by the ISIS algorithm to have a conserved secondary structure (data not shown) (Rost and Sander, 1993).

We confirmed that mutant *moag-4* was responsible for suppressing aggregation, by injecting a transgenic rescue fragment containing the genomic locus of wild-type *moag-4* into *moag-4* mutant animals (Figures 1B and 1G). We then investigated whether a gain of function or inactivation of *moag-4* was responsible for suppressing aggregation. Both RNAi and genetic deletion of *moag-4(gk513)*, hereafter referred to as *moag-4(del)*, reduced the number of aggregates similar to mutant *moag-4* (Figures 1F, 1H, and 1I). These results show that inactivation of *moag-4* suppresses the formation of polyglutamine aggregates.

MOAG-4 Acts Cell Autonomously on Protein Aggregation

Known modifiers of protein aggregation include intracellular mechanisms, involving protein folding and degradation, and extracellular mechanisms, such as excitotoxicity (Behrends et al., 2006; Garcia et al., 2007; Muchowski et al., 2000; Nollen et al., 2004; Warrick et al., 1999; Zhai et al., 2008). If MOAG-4 acts intracellularly, expression of MOAG-4 only within the same cells that express Q40::YFP should increase aggregation in the *moag-4* deletion strain. To test this possibility, we expressed MOAG-4 from the *unc-54* promoter in the *moag-4* deletion strain, which drives expression to the same subset of cells that express Q40::YFP. Expression of MOAG-4 in these cells increased the number of aggregates (Figure 1J), showing that MOAG-4 acts from within the cell.

MOAG-4 Drives Formation of Compact Misfolding Intermediates

Having demonstrated that MOAG-4 acts intracellularly to modify the formation of aggregates, we then investigated where MOAG-4 acts in this process. We excluded the possibility that aggregation was suppressed by MOAG-4 changing the expression level from the transgene promoter, by showing that wild-type Q40 animals or *moag-4* mutants expressed similar levels of YFP mRNA, protein, and polyglutamine-YFP proteins from the same promoter (Figures 2A and 2B). Another possibility is that MOAG-4 acts on an intermediate step in the aggregation pathway. In this case, inactivating MOAG-4 should lead to the accumulation of one or more aggregation intermediates. To detect aggregation intermediates, we developed a native agarose-gel electrophoresis (NAGE) assay. Lysates of *moag-4* mutant and *moag-4* deletion and wild-type polyglutamine
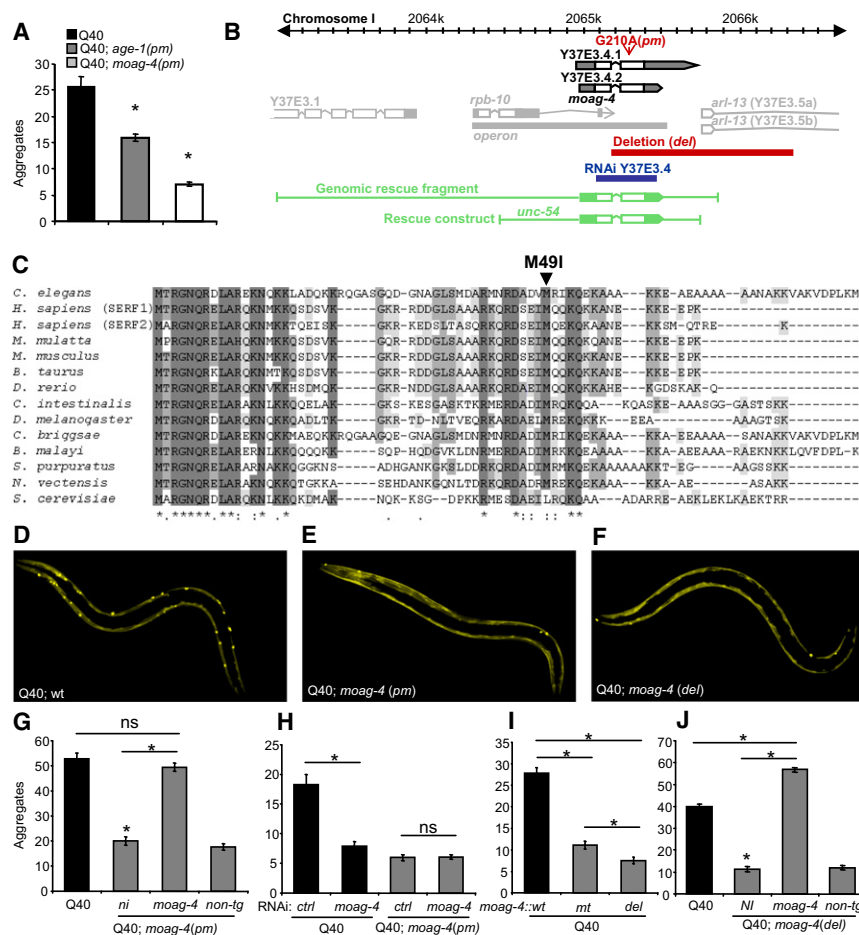
Figure 1. Inactivation of MOAG-4 Suppresses Polyglutamine Inclusion Formation

(A) Number of aggregates in Q40, Q40;*moag-4*(*pm*), and Q40;*age-1*(*pm*) mutant animals (L4 stage).

(B) Chromosomal location of the *moag-4*(Y37E3.4) gene (http://www.wormbase.org, March 2010), showing the location of the *moag-4* point mutation (*pm*), deletion (*del*), *moag-4* RNAi fragment and rescue fragment.

(C) Alignment of the *C. elegans* MOAG-4 protein with representative orthologs from two eukaryotic kingdoms including *fungi* (yeast *S. cerevisiae*) and diverse animal phyla, showing conservation of the N-terminal domain and surrounding the M49I substitution.

(D–F) Confocal images of Q40 animals with wild-type, point mutant, or deleted *moag-4*.

(G) Quantification of aggregates in Q40 animals and Q40;*moag-4*(*pm*) animals, with and without transgenic overexpression of an injected *moag-4* genomic locus rescue construct using the endogenous *moag-4* promoter (n = 13). NI denotes noninjected.

(H) Quantification of aggregates in Q40 animals and Q40;*moag-4*(*pm*) animals fed on control bacteria containing empty RNAi vector (ctrl) and expressing double-stranded RNA targeting *moag-4* (n ≥ 10).

(I) Quantification of aggregates in Q40 animals with wild-type, point mutant, or deleted *moag-4*.

(J) Quantification of aggregates in Q40 animals and Q40;*moag-4*(*del*) animals, with and without transgenic overexpression of an injected *moag-4* construct using the *unc-54* muscle promoter (n = 8). In all panels, error bars represent the standard error of the mean (SEM), *p < 0.0001, n.s. is nonsignificant; tests were one-tailed t tests. Aggregates were quantified at the L4 larval stage, except for Figure 1G, which was done in young adults. See also Figure S1.

animals were separated on a native agarose gel and the fluorescent molecules were visualized in gel by a fluorescence laser scanner. This revealed a variety of differentially migrating protein species in all Q40 animal lysates (Figure 2C), which were not detected by western blot analysis of SDS-PAGE of the same material. Also, no such forms could be observed in lysates of Q0 or Q24 animals, indicating that the formation of these species was specific for expanded polyglutamine (Figures 2C and 2D, bands 1, 3–5, 6–7, and 8–9).

In order to further characterize these intermediates, we then excised them from agarose gel after separation to analyze their SDS solubility by SDS-PAGE followed by western blotting (Figures 2E–2G). We combined this SDS-PAGE characterization with quantifying the amount of fluorescence on NAGE. This revealed that in the *moag-4* mutants there was at least a 2-fold decrease in a fraction that contained SDS-resistant aggregates and that it was retained in the slots of the gel (Figures 2C and 2D and Figure S2, band 1). Furthermore, we observed a more than 2-fold increase in two faster migrating SDS-soluble fractions (bands 3–5 and 6–7) (Figures 2C–2G, Figure S2). Lastly, and most prominently, in lysates of wild-type animals, a diffuse band of fast-migrating SDS-sensitive forms was present (Figures

2C, 2D, 2F, and 2G, bands 8–9 and Figure S2). This band was reduced by 4-fold in lysates of *moag-4* deletion strains (Figures 2C, 2D, and 2E, bands 8–9 and Figure S2). When extracted from the agarose gel and run on an SDS-PAGE gel, these species had the same size as the monomeric protein, which excluded degradation as the reason for their fast migration on the native agarose gel (Figure 2F, lanes 8 and 9). Alternatively, the difference in migration could have been caused by a more compact fold or a covalent modification that increased the net negative charge of the protein. We excluded charge as a possibility by showing that on a blue native gel, which hides the inherent protein charge by nondenaturing binding of charged Coomassie blue stain, this species still migrates faster than the more abundant monomeric species (data not shown). Our data therefore suggest that this band contains compact aggregation intermediates. As this species was nearly absent in the *moag-4* deletion strain, showing reduced aggregation, such compact aggregation intermediates appear to be on a pathway prior to aggregate formation. Together, these results suggest that the presence of MOAG-4 drives aggregation-prone proteins toward a compact conformation preceding the formation of aggregates (Figure 2H).
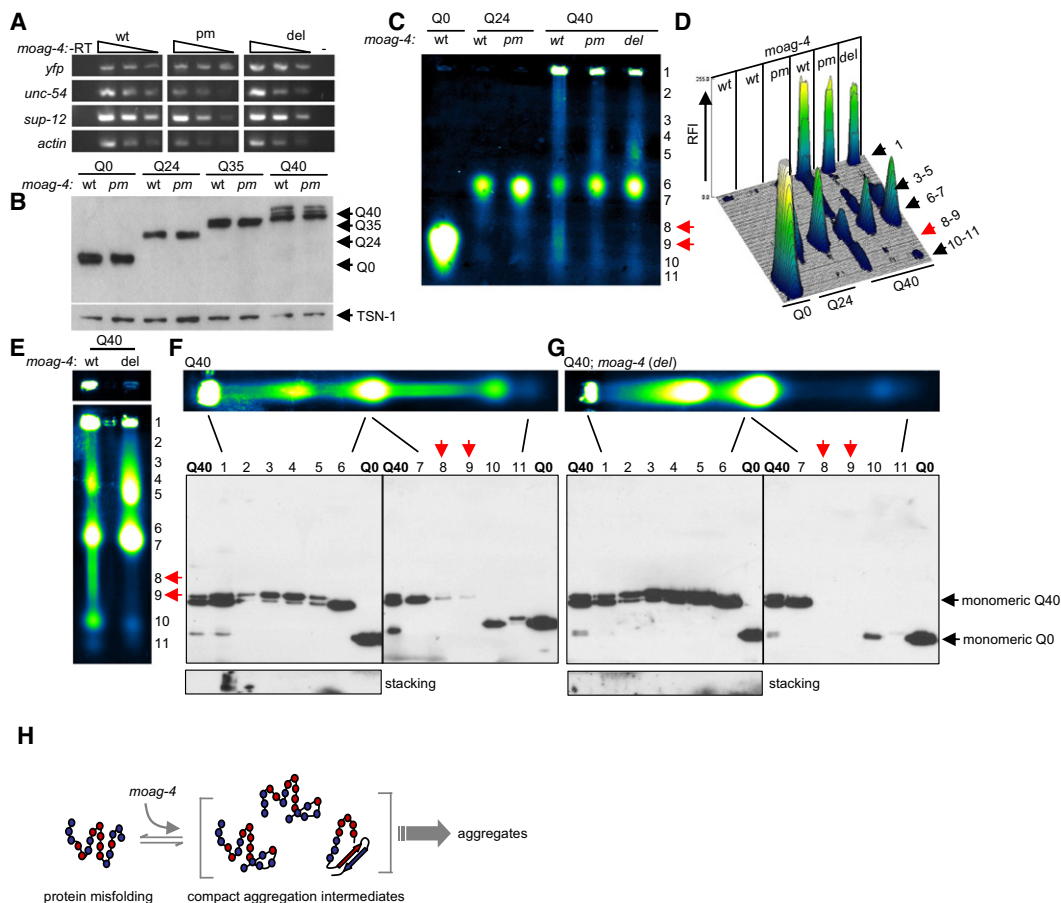
Figure 2. Inactivation of MOAG-4 Suppresses the Formation of Compact Aggregation Intermediates

(A) Analysis of *YFP*, *unc-54*, *sup-12*, and *act-4* mRNA expression in Q40;*moag-4(wt)*, Q40;*moag-4(pm)*, and Q40;*moag-4(del)* animals. It shows PCR products of cDNA dilutions (1:10, 1:20, and 1:50), a −RT control, and a control without template for all genes. *sup-12* served as a control for gene expression regulation at the X-chromosomal level. *Act-4* served as an internal expression control.

(B) Western blot analysis of denaturing SDS-PAGE separated protein lysates of Q0, Q24, Q35, and Q40 with wild-type and *pm* allele for YFP expression using GFP antibody.

(C) Native agarose gel electrophoresis (NAGE) showing in-gel fluorescence of native species of YFP and YFP-polyQ fusions in young adult, whole-animal lysates.

(D) Graphical representation of fluorescence in native agarose gel depicted in (C) indicating four differentially migrating smears (bands 1, 3–5, 6–7, and 8–9). RFI indicates relative fluorescence intensity.

(E–G) Fluorimetric scan of protein lysates of Q40 and Q40;*moag-4*(*del*) animals at day 6 separated by 1% NAGE, followed by separation of denatured agarose fragments on SDS-PAGE and western blot analysis by probing with a GFP antibody.

(H) Model for the regulation of aggregation by MOAG-4: MOAG-4 drives the formation of compact misfolding intermediates that precede aggregate formation. See also Figure S2.
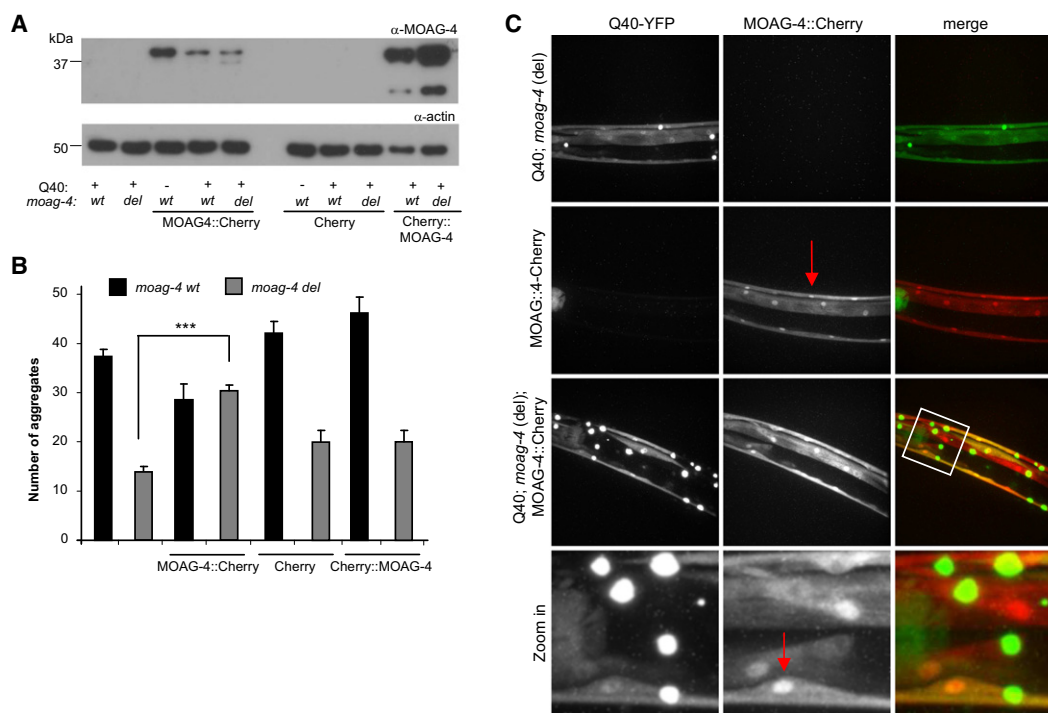
MOAG-4 Is Excluded from Polyglutamine Aggregates

To study where MOAG-4 acts in the cell, we expressed MOAG-4 fused to the red fluorescent protein mCherry (Cherry) from the *unc-54* promotor in the same cells in which Q40::YFP is expressed. Expression of the fusion protein of the correct size was confirmed by SDS-PAGE followed by western blotting using MOAG-4-specific antibodies (Figure 3A). MOAG-4 fused to cherry retained its function because animals expressing MOAG-4::Cherry, and not Cherry or a fusion of Cherry to the N terminus of MOAG-4, fully rescued the reduction in the number of aggregates in the *moag-4* deletion strain (Figure 3B). MOAG-4::Cherry showed a diffuse expression pattern in the cytosol and in cell nuclei (Figure 3C, MOAG-4::Cherry and

Figure S3). The localization of MOAG-4::Cherry was unaltered in the presence of polyglutamine aggregates and MOAG-4 did not colocalize with the aggregates (Figure 3C). These results indicate that MOAG-4 may drive aggregation by acting on soluble aggregation-prone proteins directly or by regulating a signaling pathway.

Aggregation Suppression by *moag-4* Is Independent of *daf-16* and *hsf-1*

Suppression of aggregation in *age-1* mutant animals requires the activities of both HSF-1 and DAF-16, which drive the expression of molecular chaperones that suppress aggregation. We addressed whether, similar to these IIS-compromised animals,

Figure 3. MOAG-4::Cherry Is Excluded from Polyglutamine Aggregates

(A) Western blot analysis of protein lysates of Q40, Cherry, and MOAG-4::Cherry worms with peptide polyclonal antibodies against MOAG-4 and mouse anti-actin.

(B) Quantification of the number of aggregates in Q40;*moag-4(wt),* Q40;*moag-4*(*del*), and animals transgenically expressing MOAG-4::Cherry, Cherry, or Cherry::MOAG-4 (L4). ***p = $2*10^{-12}$.

(C) Confocal images of red and green fluorescence and merged images of Q40;*moag-4(del)*, MOAG-4::Cherry, and double transgenic Q40;*moag-4(del)* × MOAG-4::Cherry worms. Lower panels show enlargements of indicated area. See text for description of arrows.

Significance was calculated using two-tailed Student's t test. In all panels, error bars represent SEM. See also Figure S3.

suppression of aggregation by deletion of *moag*-4 required HSF-1 and DAF-16 or their induced chaperones. We created double-mutant animals containing the *moag-4* deletion and an inactivating mutation in *hsf-1*(*sy441*) (*hsf-1*(*pm*)) or a deletion in *daf-16(mu86) (daf-16(del))* or by depletion of *hsf-1* or *daf-16* by RNAi. Loss of *hsf-1* or *daf-16* or both could not rescue suppression of aggregation by *moag-4* deletion (Figures 4A and 4B).
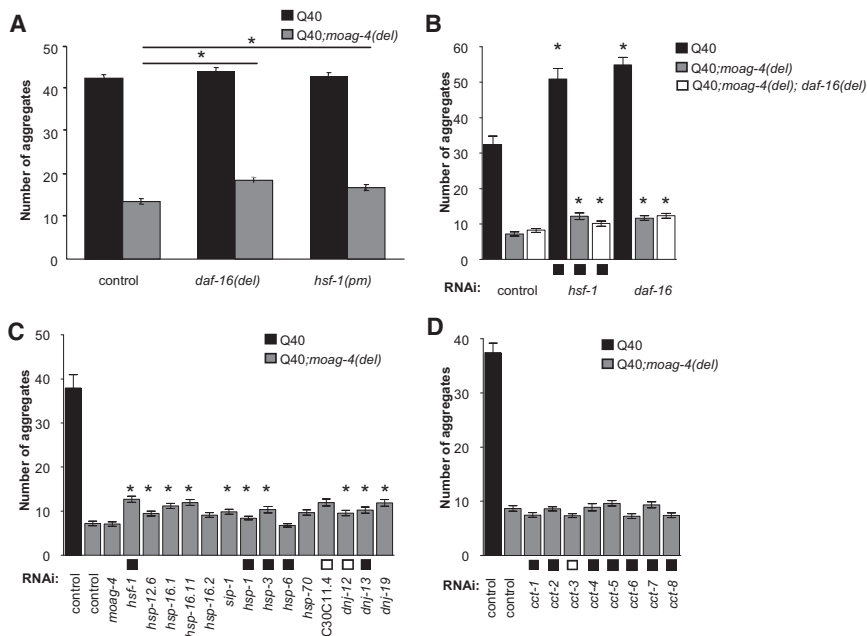
We then asked whether chaperones that have been described previously as influencing protein aggregation regulated the suppression of aggregation in the *moag-4* deletion strain (Hsu et al., 2003; Morley and Morimoto, 2004; Nollen et al., 2004). The expression of some of these chaperones is regulated by HSF-1 and DAF-16. Knockdown of these chaperones by RNAi did not rescue the suppression of aggregation in the strain lacking *moag-4* (Figures 4C and 4D). These results suggest that MOAG-4 enhances aggregation either downstream or in parallel to transcription factors and molecular chaperones that have been described previously as influencing protein aggregation in *C. elegans*.

SERF1A and SERF2 Drive Mutant Huntingtin Aggregation in Human Neuroblastoma Cell Lines

We next tested whether the human orthologs of MOAG-4, SERF1A and SERF2, also play a role in polyglutamine aggrega-

tion. We addressed their influence on the toxicity and aggregation of a mutant huntingtin exon 1 fragment with 74 polyQ repeats (Q74) in SK-N-SH neuroblastoma cells (Narain et al., 1999). We used as a control a mutant huntingtin exon 1 fragment with 23 polyQ repeats (Q23), which does not form aggregates. Overexpression of SERF1A and SERF2 significantly increased Q74 aggregation and increased cell death (Figures 5A and 5B).

Conversely, knockdown of either SERF1A or SERF2 in HEK293 cells by RNAi decreased Q74 aggregation and Q74-induced toxicity. Aggregation was suppressed without altering the levels of polyglutamine expression, as SERF 1 or SERF2 knockdown did not significantly alter the levels of the wild-type huntingtin fragment (Figures S4B–S4). These effects were also independent of autophagy and proteasomal degradation because overexpression of SERF1 or SERF2 increased mutant huntingtin aggregation in both wild-type and autophagy-deficient (*Atg5*$^{-/-}$) mouse embryonic fibroblasts (Figure 5D) and SERF1 and SERF2 overexpression did not affect the accumulation of the specific ubiquitin-proteasome substrate Ub^{G76V}-GFP (Figure 5D) or wild-type huntingtin fragment (Figure S4A). Thus, human SERF proteins regulate polyglutamine aggregation in a similar manner to MOAG-4, which indicates that this aggregation-promoting function has been evolutionarily conserved from worms to humans.

Quantification of the number of aggregates in L4 larvae.

(A) Aggregates in Q40, Q40;*moag-4(del)*, Q40;*daf-16(del)*, Q40;*moag-4(del);daf-16(del)*, Q40;*hsf-1 (pm)*, and Q40;*moag-4(del);hsf-1(pm)* (n = 40). Significance was calculated using one-tailed unpaired t test.

(B) Aggregates in Q40, Q40;*moag-4(del)*, and Q40;*daf-16(del)* fed for two generations on control, *hsf-1*, and *daf-16* RNAi foods.

(C and D) Aggregates in Q40 on control RNAi and Q40;*moag-4(del)* on control RNAi and RNAi targeting the indicated chaperones that have been described previously to modify polyglutamine aggregation in *C. elegans*.

In all panels, error bars represent SEM. Significance was calculated using two-tailed Student's t test. Asterisks indicate a significant increase in aggregation compared to control RNAi (Bonferroni corrected p value < 0.05). As an internal quality control for RNAi, squares indicate the penetrance (<50% [open] and > 50% [filled]) of all associated visible RNAi phenotypes other than aggregation.

Loss of *moag-4* Suppresses Toxicity of Polyglutamine in *C. elegans*

Expression of expanded polyglutamine in *C. elegans* body-wall muscle cells is toxic, as measured by a progressive decline in the motility of the animals during aging (Morley et al., 2002). To investigate if MOAG-4 plays a role in polyglutamine toxicity, we measured the motility of age-synchronized animals expressing Q40::YFP with or without *moag-4.* The toxicity of Q40::YFP from day 12 onward was suppressed in the *moag-4* deletion animals (Figure 6A, p < 0.05). These results suggest that the presence of MOAG-4 enhances the toxicity of polyglutamine.

Loss of *moag-4* Suppresses Aggregation and Toxicity of Amyloid-Beta and Alpha-Synuclein

To determine whether MOAG-4 is a more general regulator of proteotoxicity or whether its actions are specific for aggregation-prone polyglutamine proteins, we investigated the effects of *moag-4* inactivation in *C. elegans* models for aggregation of human amyloid-beta peptide ($A\beta_{1-42}$), alpha-synuclein, and mutant SOD1.

Ectopic expression of the human amyloid-beta peptide ($A\beta_{1-42}$) in the muscle cells of *C. elegans* results in the formation of amyloidogenic aggregates and a progressive paralysis of the worms (Link, 1995). Deletion of *moag-4* in $A\beta_{1-42}$ worms resulted in a decrease of more than 40% in the fraction of paralyzed worms over a 12 day time course (Figure 6B). To address whether suppression of paralysis in *moag-4* deletion worms was accompanied by an alteration in the amount of $A\beta_{1-42}$ seeding-competent (fibrillar) aggregates, we used an in vitro kinetic aggregation assay (Cohen et al., 2006). This assay measures the aggregation kinetics of purified $A\beta_{1-40}$ peptides, which depends on the amount of fibrillar seeding that is present in sonicated lysates of $A\beta_{1-42}$ expressing worms. Lysates of

worms with a *moag-4* deletion seeded $A\beta_{1-40}$ aggregation significantly slower than lysates of wild-type $A\beta_{1-42}$ worms (t_{50} = 30 hr versus t_{50} = 17 hr, p < 0.05), indicating that *moag-4* deletion worms contained fewer seeding-competent fibrillar $A\beta_{1-42}$ aggregates (Figure 6C). In addition, SDS-PAGE analysis of sonicated lysates of the *moag-4* deletion strain showed an alteration in the relative size distribution of $A\beta_{1-42}$ oligomers compared to wild-type worms, without lowering the total amount of $A\beta_{1-42}$ (Figure 6D and Figure S5A). In particular, subsets of the highest as well as the lowest molecular weight species, which were abundant in the wild-type lysates, were nearly absent in the *moag-4* deletion lysates, which was compensated by an increase in intermediate size oligomeric forms. Together, these results suggest that the activity of MOAG-4 normally leads to an increase in the formation of amyloidogenic conformers of $A\beta_{1-42}$.

Expression of YFP-tagged human alpha-synuclein or mutant human SOD in *C. elegans* muscle cells results in an age-dependent formation of inclusions (Gidalevitz et al., 2009; van Ham et al., 2008). Expression of alpha-synuclein and SOD in these worms resulted in an age-dependent and progressive decline in motility (Figures 6E and 6H) (Gidalevitz et al., 2009). Deletion of *moag-4* suppressed the toxicity of alpha-synuclein from day 4 onward (p < 0.05) but had no influence on the toxicity of mutant SOD (Figures 6E and 6H). Similarly, although deletion of *moag-4* did reduce the number of alpha-synuclein-YFP inclusions by ~30% (p < 0.01) without affecting the amount of alpha-synuclein-YFP expression in the worms (Figures 6F and 6G, Figure S5B), it had no effect on the number of inclusions in mutant SOD worms (Figure 6J and Figure S5C). In all, our results suggest that MOAG-4 is a general regulator of protein aggregation and proteotoxicity but it does not act on all disease-associated aggregation-prone proteins.
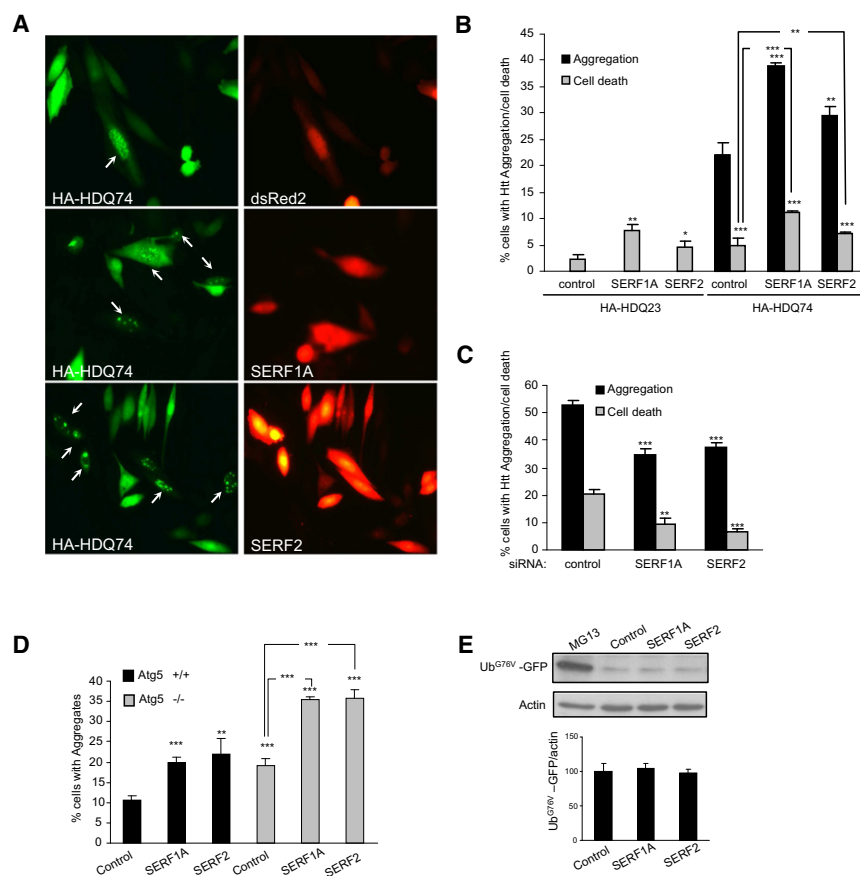
Figure 5. Human SERF1A and SERF2 Modulate the Aggregation and Toxicity of Mutant Huntingtin in Neuronal Cell Lines

(A) SK-N-SH cells transiently transfected with SERF1A or SERF2, or control (dsRed2), and HA-tagged huntingtin exon 1 (Q74) (at a 3:1 ratio) for 24 hr were labeled with anti-HA antibody to detect Q74. Q74-expressing cells with aggregates are marked by arrows.

(B) Percentage of Q23- and Q74-transfected SK-N-SH cells showing aggregation and cell death after transient transfection with SERF1A or SERF2, or control (dsRed2), and HA-tagged huntingtin exon 1 (Q23 or Q74) (at a 3:1 ratio) for 24 hr.

(C) Representative experiment of Q74 aggregation and cell death in HEK293 cells transiently transfected with siRNA targeting SERF1A or SERF2, or a nontargeting siRNA as control, and HA-tagged huntingtin exon 1 (Q74) for 48 hr. Statistics were performed by calculating odds ratios from multiple, independent triplicate experiments (see Experimental Procedures) ***$p < 0.001$; **$p < 0.01$; *$p < 0.05$.

(D) Percentage of transfected cells showing Q74 aggregation in $Atg5^{+/+}$ (wild-type) or $Atg5^{-/-}$ (Atg5 knockout) MEF cells after transient transfection with SERF1A or SERF2, or control (dsRed2), and HA-tagged huntingtin exon 1 (Q74) (at a 3:1 ratio) for 48 hr. Statistics were performed by calculating odds ratios from multiple, independent triplicate experiments (see Experimental Procedures).

(E) UbG76V-GFP levels in HeLa cells stably transfected with UbG76V-GFP after transient transfection with SERF1A or SERF2, or control (dsRed2). MG132 (proteasome inhibitor) treatment for 24 hr was used as control.

In all panels, error bars represent SEM. See also Figure S4.

Regulation of Aggregation by MOAG-4 Is Independent of Life Span

Knowing that inactivation of *age-1* suppresses polyglutamine aggregation and prolongs life span, we then asked whether inactivation of *moag-4* would also affect life span. We measured over time the survival of age-synchronized wild-type-, *age-1* mutant, and *moag-4* mutant animals. Animals with a point mutation in *moag-4*, which suppresses aggregation to a similar extent as the *moag-4* deletion, do not show an effect on life span (Figure 7). These results provide evidence that the aggregation regulatory activities of *moag-4* are uncoupled from life-span regulation.
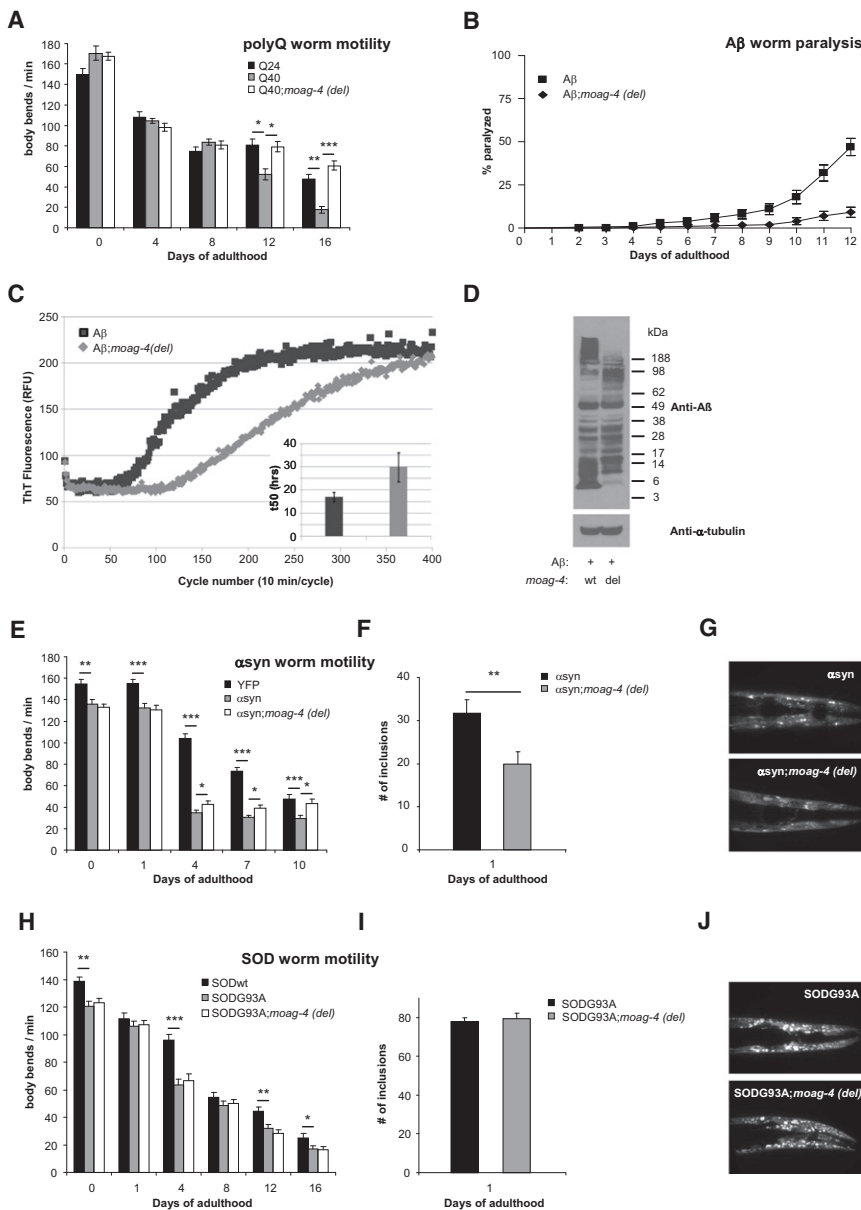
DISCUSSION

Fibrillar aggregates are thought to arise from toxic aggregation-prone proteins when the activities of other protein quality control mechanisms decline or are functionally impaired, which may occur during aging or in disease (Kaganovich et al., 2008; Williams and Paulson, 2008). Here we describe a previously unidentified modifier, MOAG-4, as a positive regulator of aggregate formation in *C. elegans* and human cell models for neurodegenerative disease. In animals expressing polyglut-

amine, MOAG-4 induces a conformational change in aggregation-prone proteins preceding the formation of aggregates.

We have identified MOAG-4 as a regulator of proteotoxicity in transgenic disease models. The natural function of MOAG-4 in the absence of these exogenous proteins remains to be investigated, but we would like to propose three possible functions.

One possibility is that MOAG-4 acts as an inhibitor of a stress-response pathway, similar to the IIS pathway, and that deletion of MOAG-4 induces the expression of downstream targets that suppress proteotoxicity (Cohen et al., 2006, 2009; Hsu et al., 2003; Morley and Morimoto, 2004). As suggested by our findings, these targets would then be induced independently of the IIS transcription factors DAF-16 and HSF-1. Moreover, these targets would involve a different subset than those that have previously been described to suppress proteotoxicity, indicating that MOAG-4 would act through a previously unexplored stress-response pathway.

Second, MOAG-4 could act positively on aggregation, either as a component of a pathway or by direct interaction with the aggregation-prone proteins. For example, MOAG-4 may normally act in an endogenous amyloid pathway, such as the one that is used for hormone peptide storage and secretion
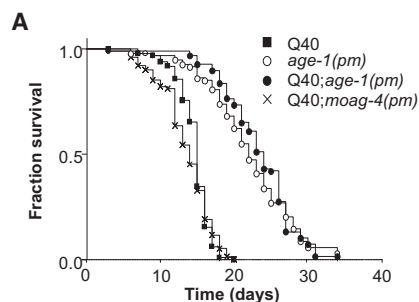
(Maji et al., 2009). Aggregation-prone disease proteins could then be anomalously recognized as targets and hijack this hormone peptide storage and secretion system and cause toxicity from within or from outside the cell.

Finally, MOAG-4 could be part of a quality control pathway that drives toxic, aggregation-prone proteins into aggregates for storage (Kaganovich et al., 2008). Increased proteotoxic stress, such as the constitutive presence of aggregation-prone disease proteins, may saturate this pathway and lead to the accumulation of toxic intermediates. Our finding that MOAG-4

is involved in the formation of such aggregation intermediates would then explain why loss of MOAG-4 suppresses toxicity. Further studies are needed to explore these and other possible mechanisms.

Previously, other factors have been identified that enhance polyglutamine protein aggregation. These include the SH3-domain GRB2-like 3 (SH3GL3) and the G protein-coupled receptor kinase interacting-protein 1 (GIT1), which act by an unknown mechanism, and components of the microtubule network that is thought to be involved in transport of

A

of offspring. The strains used or generated are described in the Extended Experimental Procedures.

B

Strain	Mean +/- SEM in days	versus	Mean +/- SEM in days	P-value
age-1(pm)	20.3 +/- 0.6	Q40;*age-1(pm)*	22.9 +/- 0.5	= ns
		Q40	14.5 +/- 0.3	< 0.0001
Q40;*moag-4(pm)*	13.3 +/- 0.3	Q40	14.5 +/- 0.3	= ns

aggregation-prone proteins toward aggregates (Goehler et al., 2004; Muchowski et al., 2002; Sittler et al., 1998). It will be interesting to establish how MOAG-4 functionally relates to these modifiers.

The human orthologs of MOAG-4, SERF2 and SERF1A, are ubiquitously expressed, consistent with a role in a general cellular pathway. *SERF1A* was first identified as a genetic modifier of spinal muscular atrophy (SMA), but its function and how it enhances the severity of this disease is still unknown (Scharf et al., 1998). Based on our findings that these human orthologs of MOAG-4 similarly modify protein aggregation, it is possible that protein misfolding plays a role in enhancing the SMA phenotype.

In all, the *moag-4* gene is part of a pathway regulating age-related proteotoxicty. Further exploration of this pathway will broaden our understanding of how cells cope with the constant challenges on protein stability imposed by intracellular and extracellular environmental perturbations and in disease.

Furthermore, as deletion of *moag-4* does not affect the viability of the organism and *SERF2* and *SERF1* are evolutionarily highly conserved human orthologs of *moag-4*, this pathway may provide a new target for therapeutic intervention in the early molecular events of aging-associated neurodegenerative diseases. Our findings suggest that, apart from activating HSF-1-regulated molecular chaperones, proteasomal degradation, or autophagy, an alternative strategy to ameliorate the toxic effects of aggregation-prone proteins in disease could be to intervene in this pathway.

EXPERIMENTAL PROCEDURES

Media and Strains

Standard conditions were used for *C. elegans* propagation at 20°C (Brenner, 1974). Animals were synchronized by hypochlorite bleaching, hatched overnight in M9 buffer, and subsequently cultured on NGM agar plates seeded with OP50. On day 3 after synchronization, animals were placed on NGM plates containing 5-Fluoro-2′deoxy-uridine (FUDR) to inhibit growth

was identified by single-nucleotide polymorphism (SNP) mapping (Wicks et al., 2001) to a region between base 1,983,175 and 2,080,838 on linkage group I. All exons of 16 remaining candidate genes in that region were sequenced to identify the mutation in Y37E3.4. Suppression of aggregation was rescued by reintroduction into NL4436 of a genomic construct spanning 1 kb upstream to 300 bp downstream of the Y37E3.3, Y37E3.4, and Y37E3.5 containing operon. The operon was amplified by nested PCR and was coinjected with pJKL449.1[P(*myo-2::GFP*)] as a coinjection marker.

RNA Isolation and Reverse Transcriptase PCR

Total RNA was extracted from L4 synchronized animals using Trizol reagent (Invitrogen, Breda, the Netherlands) according to the manufacturer's instructions. cDNA was made from 2 μg total *C. elegans* RNA using Ready-To-Go First Strand Synthesis Beads (GE Healthcare, Leiderdorp, The Netherlands), including a control without reverse transcriptase (-RT) for all strains indicated. Serial dilutions of the cDNA (1:10, 1:20, and 1:50) and the -RT control were amplified using PCR with cycle numbers varying between 25 and 31 for optimal detection of the PCR product. Samples were run on 2.5% agarose-gels stained with ethidium bromide, imaged with a UV scanner, and analyzed using Image J software.

Quantification of Aggregates

The number of aggregates present in whole animals was counted using a fluorescence dissection stereomicroscope (Leica Microsystems, Wetzlar, Germany) at a nominal magnification of ~100×. At least twenty animals were counted, unless stated otherwise. Microsoft Excel Student's t test was used to calculate p values. All tests were two-tailed unpaired unless otherwise stated.

Immunoblotting Analysis

C. elegans protein extracts were prepared from whole animal frozen pellets in PBS containing proteinase inhibitors (Roche, Indianapolis, USA) by using Fastprep24 (MP, Solon, USA). Samples were boiled for 5 min with sample buffer containing SDS and DTT and separated using 10% SDS-PAGE. Proteins were transferred to PVDF membranes by semi-dry blotting. Primary antibodies used were anti-GFP (monoclonal [JL-8], polyclonal [full-length GFP, Clontech, Mountainview, CA, USA]), anti-RFP (polyclonal, Clontech), anti-tubulin (monoclonal B-5-1-2, Sigma Aldrich, St. Louis, MO, USA), anti-actin (monoclonal C4, MP Biomedicals), and custom-made polyclonal peptide antibodies against MOAG-4. Goat anti-mouse and goat anti-rabbit IgG-HRP (BioRad, Hercules, CA, USA) were used as secondary antibodies. Antibody binding was visualized by chemiluminescence (ECL Lumi-Light, Roche, Germany).

Creation of Transgenic Strains

Microinjection was used to create new transgenic strains as described. Unless mentioned otherwise, animals were outcrossed to N2 at least four times.

EMS Mutagenesis and Mapping

Mutagenesis was performed using standard *C. elegans* ethyl methanesulfonate (EMS) methodology (Jorgensen and Mango, 2002). Eight thousand mutagenized genomes were screened for suppressors of aggregation. *moag-4(pk2185)*

Protein Separation on Agarose Gel

Native protein extract was loaded with native loading buffer (working concentration of 0.0625 M tris, 10% glycerol, and bromophenol blue) on horizontal 1% agarose gel (running buffer 25 mM tris, 0.19 M glycine [pH 8.3]). Gels were run for 14 hr at 4°C and analyzed using a laser scanner (Molecular imager FX, Bio-Rad) with excitation at 488 nm and detection of emission at 530 nm. Image analysis was performed using ImageJ software. Excised agarose fractions were denatured and liquefied by boiling in SDS sample buffer containing DTT and loaded on SDS-PAGE gel while liquid for subsequent western blotting. Quantification of different protein species were calculated as means of three independent experiments. Error bars represent standard error of the mean (SEM).

In Vitro Aβ_{1-40} Kinetic Aggregation Assay with Worm PDS

Sonicated post-debris supernatant (PDS) of worms was mixed with monomerized synthetic Aβ_{1-40} peptide to a final concentration of 10 μM in phosphate buffer (50 mM Na-phosphate, 150 mM NaCl, pH 7.4) containing ThT (20 μM). Aliquots (100 μl) in a 96-well microplate (Costar black, clear bottom) were read with a TECAN fluorescence microplate reader (Tecan Group Ltd) at 37°C. Half-maximal fluorescence time points (t_{50}) were defined as the time point at which ThT fluorescence reached the midpoint between pre- and post-aggregation baselines (see also Extended Experimental Procedures for a detailed description).

Confocal Laser Scanning Microscopy

Transgenic animals were mounted on 2% agarose pads containing 40 mM NaN$_3$ as anesthetic on glass microscope slides. Fluorescence images were captured with a confocal microscope (TCS SP2 AOBS or SOLAMERE, and Leica Microsystems, Mannheim, Germany) using a 40× oil immersion objective (HCX PL APO CS, Leica). Images shown are maximal projections of Z stacks.

Life-Span Assays

Life-span assays were carried out by growing L4 stage synchronized animals on NGM agar plates containing FUDR. Animals were grown at 20°C. Life spans were started from 100 L4 stage animals per strain on FUDR-containing agar plates seeded with OP50 and allowed to grow at 20°C. At each time point, the number of surviving animals was counted, as determined by movement and response to nose touch. Animals that disappeared during the assay or crawled out of the plates were excluded. Analysis was performed using Graphpad Prism (GraphPad Software, San Diego, CA, USA).

Motility Assay

At different ages, animals were placed in a drop of M9 and were allowed to recover for 1 min after which the number of body bends was counted for 1 min. At least 12 animals were counted per experiment, unless stated otherwise, and the data from three independent experiments were combined. Statistical analyses were performed in Graphpad Prism (GraphPad Software) (Gidalevitz et al., 2009).

Paralysis Assay

Paralysis assays were performed by growing L4 stage synchronized animals on agar plates containing FUDR. To avoid developmental defects of the vulva, animals were grown at 15°C until the first day of adulthood, after which they were moved to 20°C. Each individual experiment was started from 100 L4 stage animals per strain. Animals were tested every day for 12 consecutive days for paralysis by tapping their noses and tail-prodding with a platinum wire as described previously (Cohen et al., 2006). Worms that moved their noses but failed to move their bodies were scored as "paralyzed." Analysis was performed using Graphpad Prism (GraphPad Software).

RNAi Experiments

RNAi experiments were performed on NGM agar plates containing 1 mM IPTG and 50 mg/ml ampicillin that were seeded with RNAi bacteria induced with IPTG to produce dsRNA. Animals synchronized by hypochlorite bleaching were grown on RNAi plates and used for the experiments. The RNAi clones used were verified by sequencing the insert using L4440 primers and subsequent BLAST analysis to confirm the correct sequence.

Mammalian Cell Culture

Human neuroblastoma cell line (SK-N-SH), human embryonal kidney cell line (HEK293), and wild-type Atg5 ($Atg5^{+/+}$) and Atg5-deficient ($Atg5^{-/-}$) mouse embryonic fibroblasts (MEFs) (kindly given by N. Mizushima) were maintained in Dulbecco's modified Eagle's medium supplemented with 10% fetal bovine serum, 100 units/ml penicillin/streptomycin, and 2 mM L-glutamine (Sigma) at 37°C, 5% CO2 (Mizushima et al., 2001).

Cells were transfected using Lipofectamine or reagent (Invitrogen) according to the manufacturer's protocol and fixed with 4% paraformaldehyde (Sigma) after 24–48 hr post-transfection, HA-HDQ74 and HA-HDQ23 expression detected using an anti-HA antibody (12CA5, Covance) and fluorophore-conjugated secondary antibody (Alexa Fluor [green] anti-mouse; Molecular Probes), and mounted in Citifluor (Citifluor Ltd.) containing 4′,6-dia-midino-2-phenylindole (DAPI; 3 μg/ml; Sigma-Aldrich).

Quantification of Aggregate Formation and Cell Death

Aggregate formation and nuclear morphology were assessed using a fluorescence microscope. Double-expressing cells with both red (SERF proteins) and green (HA-tagged HDQ74 or HDQ23) fluorescence were scored for cell death and aggregation. Approximately 200 cells per coverslip were selected and the number of cells with aggregates was counted. The experiments were performed blinded and in triplicate and repeated at least twice. Cells were considered dead if the DAPI-stained nuclei showed apoptotic morphology (fragmentation or pyknosis).

RNA Interference in Human Cells

HEK293 cells were transfected with HA-HDQ74 along with SERF1A, SERF2, or nontargeting siRNA as control (Dharmacon, cat. no. D-001210-01) for 48 hr using Lipofectamine 2000 (Invitrogen) according to the manufacturer's protocol.

The final siRNA concentration was 50 nM. Cells were fixed after transfection, immunolabeled, and analyzed by fluorescence microscopy.

Pooled estimates for changes in aggregate formation or cell death resulting from perturbations assessed in multiple experiments were calculated as odds ratios (OR; the ratios of the proportion of abnormal/normal cells in different experimental conditions) with 95% confidence intervals as described (Wyttenbach et al., 2001). Significance levels for comparisons between groups were determined with t tests.

Bioinformatic Analysis

Orthologs were identified using protein BLAST search and aligned with T-Coffee multiple sequence alignment tool (Notredame et al., 2000).

SUPPLEMENTAL INFORMATION

Supplemental Information includes Extended Experimental Procedures and five figures and can be found with this article online at doi:10.1016/j.cell.2010.07.020.

REFERENCES

Arrasate, M., Mitra, S., Schweitzer, E.S., Segal, M.R., and Finkbeiner, S. (2004). Inclusion body formation reduces levels of mutant huntingtin and the risk of neuronal death. Nature *431*, 805–810.

Behrends, C., Langer, C.A., Boteva, R., Bottcher, U.M., Stemp, M.J., Schaffar, G., Rao, B.V., Giese, A., Kretzschmar, H., Siegers, K., and Hartl, F.U. (2006). Chaperonin TRiC promotes the assembly of polyQ expansion proteins into nontoxic oligomers. Mol. Cell *23*, 887–897.

Brenner, S. (1974). The genetics of Caenorhabditis elegans. Genetics *77*, 71–94.

Bukau, B., Weissman, J., and Horwich, A. (2006). Molecular chaperones and protein quality control. Cell *125*, 443–451.

Caughey, B., and Lansbury, P.T. (2003). Protofibrils, pores, fibrils, and neurodegeneration: separating the responsible protein aggregates from the innocent bystanders. Annu. Rev. Neurosci. *26*, 267–298.

Chiti, F., and Dobson, C.M. (2006). Protein misfolding, functional amyloid, and human disease. Annu. Rev. Biochem. *75*, 333–366.

Cohen, E., and Dillin, A. (2008). The insulin paradox: aging, proteotoxicity and neurodegeneration. Nat. Rev. Neurosci. *9*, 759–767.

Cohen, E., Bieschke, J., Perciavalle, R.M., Kelly, J.W., and Dillin, A. (2006). Opposing activities protect against age-onset proteotoxicity. Science *313*, 1604–1610.

Cohen, E., Paulsson, J.F., Blinder, P., Burstyn-Cohen, T., Du, D., Estepa, G., Adame, A., Pham, H.M., Holzenberger, M., Kelly, J.W., et al. (2009). Reduced IGF-1 signaling delays age-associated proteotoxicity in mice. Cell *139*, 1157–1169.

Garcia, S.M., Casanueva, M.O., Silva, M.C., Amaral, M.D., and Morimoto, R.I. (2007). Neuronal signaling modulates protein homeostasis in Caenorhabditis elegans post-synaptic muscle cells. Genes Dev. *21*, 3006–3016.

Gidalevitz, T., Krupinski, T., Garcia, S., and Morimoto, R.I. (2009). Destabilizing protein polymorphisms in the genetic background direct phenotypic expression of mutant SOD1 toxicity. PLoS Genet. *5*, e1000399.

Goedert, M., and Spillantini, M.G. (2006). A century of Alzheimer's disease. Science *314*, 777–781.

Goehler, H., Lalowski, M., Stelzl, U., Waelter, S., Stroedicke, M., Worm, U., Droege, A., Lindenberg, K.S., Knoblich, M., Haenig, C., et al. (2004). A protein interaction network links GIT1, an enhancer of huntingtin aggregation, to Huntington's disease. Mol. Cell *15*, 853–865.

Goldberg, A.L. (2003). Protein degradation and protection against misfolded or damaged proteins. Nature *426*, 895–899.

Haass, C., and Selkoe, D.J. (2007). Soluble protein oligomers in neurodegeneration: lessons from the Alzheimer's amyloid beta-peptide. Nat. Rev. Mol. Cell Biol. *8*, 101–112.

Hsu, A.L., Murphy, C.T., and Kenyon, C. (2003). Regulation of aging and age-related disease by DAF-16 and heat-shock factor. Science *300*, 1142–1145.

Jorgensen, E.M., and Mango, S.E. (2002). The art and design of genetic screens: caenorhabditis elegans. Nat. Rev. Genet. *3*, 356–369.

Kaganovich, D., Kopito, R., and Frydman, J. (2008). Misfolded proteins partition between two distinct quality control compartments. Nature *454*, 1088–1095.

Kayed, R., Head, E., Thompson, J.L., McIntire, T.M., Milton, S.C., Cotman, C.W., and Glabe, C.G. (2003). Common structure of soluble amyloid oligomers implies common mechanism of pathogenesis. Science *300*, 486–489.

Kitamura, A., Kubota, H., Pack, C.G., Matsumoto, G., Hirayama, S., Takahashi, Y., Kimura, H., Kinjo, M., Morimoto, R.I., and Nagata, K. (2006). Cytosolic chaperonin prevents polyglutamine toxicity with altering the aggregation state. Nat. Cell Biol. *8*, 1163–1170.

Kopito, R.R. (2000). Aggresomes, inclusion bodies and protein aggregation. Trends Cell Biol. *10*, 524–530.

Link, C.D. (1995). Expression of human beta-amyloid peptide in transgenic Caenorhabditis elegans. Proc. Natl. Acad. Sci. USA *92*, 9368–9372.

Maji, S.K., Perrin, M.H., Sawaya, M.R., Jessberger, S., Vadodaria, K., Rissman, R.A., Singru, P.S., Nilsson, K.P., Simon, R., Schubert, D., et al. (2009). Functional amyloids as natural storage of peptide hormones in pituitary secretory granules. Science *325*, 328–332.

Mizushima, N., Yamamoto, A., Hatano, M., Kobayashi, Y., Kabeya, Y., Suzuki, K., Tokuhisa, T., Ohsumi, Y., and Yoshimori, T. (2001). Dissection of autophagosome formation using Apg5-deficient mouse embryonic stem cells. J. Cell Biol. *152*, 657–668.

Morley, J.F., and Morimoto, R.I. (2004). Regulation of longevity in Caenorhabditis elegans by heat shock factor and molecular chaperones. Mol. Biol. Cell *15*, 657–664.

Morley, J.F., Brignull, H.R., Weyers, J.J., and Morimoto, R.I. (2002). The threshold for polyglutamine-expansion protein aggregation and cellular toxicity is dynamic and influenced by aging in Caenorhabditis elegans. Proc. Natl. Acad. Sci. USA *99*, 10417–10422.

Muchowski, P.J., Schaffar, G., Sittler, A., Wanker, E.E., Hayer-Hartl, M.K., and Hartl, F.U. (2000). Hsp70 and hsp40 chaperones can inhibit self-assembly of polyglutamine proteins into amyloid-like fibrils. Proc. Natl. Acad. Sci. USA *97*, 7841–7846.

Muchowski, P.J., Ning, K., D'Souza-Schorey, C., and Fields, S. (2002). Requirement of an intact microtubule cytoskeleton for aggregation and inclusion body formation by a mutant huntingtin fragment. Proc. Natl. Acad. Sci. USA *99*, 727–732.

Nagai, Y., Inui, T., Popiel, H.A., Fujikake, N., Hasegawa, K., Urade, Y., Goto, Y., Naiki, H., and Toda, T. (2007). A toxic monomeric conformer of the polyglutamine protein. Nat. Struct. Mol. Biol. *14*, 332–340.

Narain, Y., Wyttenbach, A., Rankin, J., Furlong, R.A., and Rubinsztein, D.C. (1999). A molecular investigation of true dominance in Huntington's disease. J. Med. Genet. *36*, 739–746.

Nollen, E.A., Salomons, F.A., Brunsting, J.F., Want, J.J., Sibon, O.C., and Kampinga, H.H. (2001). Dynamic changes in the localization of thermally unfolded nuclear proteins associated with chaperone-dependent protection. Proc. Natl. Acad. Sci. USA *98*, 12038–12043.

Nollen, E.A., Garcia, S.M., van Haaften, G., Kim, S., Chavez, A., Morimoto, R.I., and Plasterk, R.H. (2004). Genome-wide RNA interference screen identifies previously undescribed regulators of polyglutamine aggregation. Proc. Natl. Acad. Sci. USA *101*, 6403–6408.

Notredame, C., Higgins, D.G., and Heringa, J. (2000). T-Coffee: A novel method for fast and accurate multiple sequence alignment. J. Mol. Biol. *302*, 205–217.

Ofran, Y., and Rost, B. (2003). Predicted protein-protein interaction sites from local sequence information. FEBS Lett. *544*, 236–239.

Ofran, Y., Mysore, V., and Rost, B. (2007). Prediction of DNA-binding residues from sequence. Bioinformatics *23*, i347–i353.

Ogg, S., Paradis, S., Gottlieb, S., Patterson, G.I., Lee, L., Tissenbaum, H.A., and Ruvkun, G. (1997). The Fork head transcription factor DAF-16 transduces insulin-like metabolic and longevity signals in C. elegans. Nature *389*, 994–999.

Ravikumar, B., Vacher, C., Berger, Z., Davies, J.E., Luo, S., Oroz, L.G., Scaravilli, F., Easton, D.F., Duden, R., O'Kane, C.J., and Rubinsztein, D.C. (2004). Inhibition of mTOR induces autophagy and reduces toxicity of polyglutamine expansions in fly and mouse models of Huntington disease. Nat. Genet. *36*, 585–595.

Rost, B., and Sander, C. (1993). Prediction of protein secondary structure at better than 70% accuracy. J. Mol. Biol. *232*, 584–599.

Rubinsztein, D.C. (2006). The roles of intracellular protein-degradation pathways in neurodegeneration. Nature *443*, 780–786.

Sanchez, I., Mahlke, C., and Yuan, J. (2003). Pivotal role of oligomerization in expanded polyglutamine neurodegenerative disorders. Nature *421*, 373–379.

Saudou, F., Finkbeiner, S., Devys, D., and Greenberg, M.E. (1998). Huntingtin acts in the nucleus to induce apoptosis but death does not correlate with the formation of intranuclear inclusions. Cell *95*, 55–66.

Schaffar, G., Breuer, P., Boteva, R., Behrends, C., Tzvetkov, N., Strippel, N., Sakahira, H., Siegers, K., Hayer-Hartl, M., and Hartl, F.U. (2004). Cellular toxicity of polyglutamine expansion proteins: Mechanism of transcription factor deactivation. Mol. Cell *15*, 95–105.

Scharf, J.M., Endrizzi, M.G., Wetter, A., Huang, S., Thompson, T.G., Zerres, K., Dietrich, W.F., Wirth, B., and Kunkel, L.M. (1998). Identification of a candidate modifying gene for spinal muscular atrophy by comparative genomics. Nat. Genet. *20*, 83–86.

Scherzinger, E., Lurz, R., Turmaine, M., Mangiarini, L., Hollenbach, B., Hasenbank, R., Bates, G.P., Davies, S.W., Lehrach, H., and Wanker, E.E. (1997). Huntingtin-encoded polyglutamine expansions form amyloid-like protein aggregates in vitro and in vivo. Cell *90*, 549–558.

Sittler, A., Walter, S., Wedemeyer, N., Hasenbank, R., Scherzinger, E., Eickhoff, H., Bates, G.P., Lehrach, H., and Wanker, E.E. (1998). SH3GL3 associates with the Huntingtin exon 1 protein and promotes the formation of polygln-containing protein aggregates. Mol. Cell *2*, 427–436.

Spillantini, M.G., and Goedert, M. (2000). The alpha-synucleinopathies: Parkinson's disease, dementia with Lewy bodies, and multiple system atrophy. Ann. N Y Acad. Sci. *920*, 16–27.

Tam, S., Geller, R., Spiess, C., and Frydman, J. (2006). The chaperonin TRiC controls polyglutamine aggregation and toxicity through subunit-specific interactions. Nat. Cell Biol. *8*, 1155–1162.

Tissenbaum, H.A., and Ruvkun, G. (1998). An insulin-like signaling pathway affects both longevity and reproduction in Caenorhabditis elegans. Genetics *148*, 703–717.

van Ham, T.J., Thijssen, K.L., Breitling, R., Hofstra, R.M., Plasterk, R.H., and Nollen, E.A. (2008). C. elegans model identifies genetic modifiers of alpha-synuclein inclusion formation during aging. PLoS Genet. *4*, e1000027.

Warrick, J.M., Chan, H.Y., Gray-Board, G.L., Chai, Y., Paulson, H.L., and Bonini, N.M. (1999). Suppression of polyglutamine-mediated neurodegeneration in Drosophila by the molecular chaperone HSP70. Nat. Genet. *23*, 425–428.

Wicks, S.R., Yeh, R.T., Gish, W.R., Waterston, R.H., and Plasterk, R.H. (2001). Rapid gene mapping in Caenorhabditis elegans using a high density polymorphism map. Nat. Genet. *28*, 160–164.

Williams, A.J., and Paulson, H.L. (2008). Polyglutamine neurodegeneration: protein misfolding revisited. Trends Neurosci. *31*, 521–528.

Wyttenbach, A., Swartz, J., Kita, H., Thykjaer, T., Carmichael, J., Bradley, J., Brown, R., Maxwell, M., Schapira, A., Orntoft, T.F., et al. (2001). Polyglutamine expansions cause decreased CRE-mediated transcription and early gene expression changes prior to cell death in an inducible cell model of Huntington's disease. Hum. Mol. Genet. *10*, 1829–1845.

Yamamoto, A., Lucas, J.J., and Hen, R. (2000). Reversal of neuropathology and motor dysfunction in a conditional model of Huntington's disease. Cell *101*, 57–66.

Zhai, R.G., Zhang, F., Hiesinger, P.R., Cao, Y., Haueter, C.M., and Bellen, H.J. (2008). NAD synthase NMNAT acts as a chaperone to protect against neurodegeneration. Nature *452*, 887–891.